Analytically solvable prolate-oblate shape phase transitional description within the SU(3) limit of the interacting boson model

Yu Zhang, Feng Pan, Yu-Xin Liu, Yan-An Luo, and J. P. Draayer

Phys. Rev. C **85**, 064312 — Published 12 June 2012

DOI: 10.1103/PhysRevC.85.064312

Analytically solvable prolate-oblate shape phase transitional description within the SU(3) limit of the interacting boson model

Yu Zhang,[1] Feng Pan,[1,2] Yu-Xin Liu,[3,4] Yan-An Luo,[5] and J. P. Draayer [2]

[1]*Department of Physics, Liaoning Normal University, Dalian 116029, China*

[2]*Department of Physics and Astronomy, Louisiana State University, Baton Rouge, Louisiana 70803-4001, USA*

[3]*Department of Physics and the State Key Laboratory of Nuclear Physics and Technology, Peking University, Beijing 100871, China*

[4]*Center of Theoretical Nuclear Physics, National Laboratory of Heavy Ion Accelerator, Lanzhou 730000, China*

[5]*School of Physics, Nankai University, Tianjin 300071, China*

(Dated: May 31, 2012)

Abstract

A novel analytically solvable prolate-oblate shape phase transitional description for the SU(3) limit of the interacting boson model is investigated for finite-N as well as in the large-N classical limit. It is shown that the ground state shape phase transition is of first order due to level crossing. Through a comparison of the theoretical predictions with available experimental data for even-even ^{180}Hf, $^{182-186}$W, $^{188-190}$Os, and $^{192-198}$Pt, it is shown that this simple novel description is suitable for a description of the prolate-oblate shape phase transition in these nuclei.

PACS numbers: 21.60.Fw, 21.60.Ev, 05.70.Fh, 21.10.Re

I. INTRODUCTION

Shape phase transitions in nuclei have attracted a lot of interest from both experimental and theoretical perspectives [1–29]. Theoretically, the interacting boson model (IBM) [5], which provides direct correspondence between nuclear shapes and dynamical symmetries, may be the most frequently used model for studying shape phase transitions. Various nuclear shape phase transitions can be explored within transitional patterns among different symmetries in the IBM, in which at least two of the three dynamical symmetries, U(5), SU(3) and O(6), are involved [5]. For example, the phase transition from spherical to axially deformed shape is characterized as the U(5)-SU(3) transition; the phase transition from spherical to the γ-unstable motion is described by the U(5)-O(6) transition; and the phase transition from prolate to oblate shape is often described by the SU(3)-O(6)-$\overline{\text{SU(3)}}$ transition [6, 22, 23]. It should be noted that the prolate phase and the oblate phase in the SU(3)-O(6)-$\overline{\text{SU(3)}}$ transitional description are described by the SU(3) and the $\overline{\text{SU(3)}}$ symmetry respectively, in which the O(6) limit emerges exactly at the critical point [6]. Since the $\overline{\text{SU(3)}}$ generators can be constructed from the corresponding SU(3) generators with a phase change in the s-boson operators in the IBM [30, 31], dynamical structures in the two limiting cases are the same except a sign change in the quadrupole operator [6, 25].

It was shown previously that triaxial shape phase in nuclei may be described by a model Hamiltonian with higher order terms. For example, the $[d^\dagger \times d^\dagger \times d^\dagger]^{(3)} \cdot [\tilde{d} \times \tilde{d} \times \tilde{d}]^{(3)}$ type interaction can induce a stable triaxial shape [32]; the $[\hat{Q}' \times \hat{Q}' \times \hat{Q}']^{(0)}$ term may give rise to a rotational spectrum within the O(6) limit [33], where $\hat{Q}'_q = [s^\dagger \times \tilde{d} + d^\dagger \times \tilde{s}]^{(2)}_q$ are generators of the O(6) group; a Hamiltonian involving three- and four-body interactions in the SU(3) limit can generate a spectrum of the asymmetric rotor [34], which was based on previous description of the asymmetric rotor in the $SU(3)$ shell model scheme [35–40]. As shown in these studies, the high-order interactions greatly enrich phase structures in the model even within the dynamical symmetry limit.

In this article, as a simple alternative description of the prolate-oblate shape phase transition in the IBM, the oblate shape phase is considered to be caused by a three-body interaction within the SU(3) limit [34, 41–43]. Specifically, the prolate-oblate shape phase transitional patterns are investigated within this framework. In Sec. II, the oblate shape phase generated by the three-body interaction within the SU(3) limit is discussed, and a schematic Hamiltonian for describing the prolate-oblate shape phase transition is proposed.

In Sec. III, the prolate-oblate shape phase transition in the classical limit is explored. In Sec. IV, the correspondence between two different descriptions of the shape variables, namely the shape variables determined from the coherent state theory and those determined from the SU(3) correspondence, is discussed. The prolate-oblate shape phase transition in a finite boson system is investigated in detail. In Sec. V, evolutions of some observables with variation of the control parameter in the model are considered. Comparisons of the theoretical results of some quantities with the corresponding experimental data are made. A summary is given in Sec. VI.

II. SU(3) SYMMETRY IN THE IBM AND SPECTRA IN THE OBLATE

A Hamiltonian in the IBM framework is constructed from two kinds of boson operators; namely, a s-boson with $J^\pi = 0^+$ and a d-boson with $J^\pi = 2^+$. The total boson number N is taken as the number of valence particle (or hole) pairs in a nucleus. The dynamical symmetry limits in the IBM are characterized by three different chains of the U(6) group [5]:

$$\mathrm{U}(6) \supset \mathrm{U}(5) \supset \mathrm{O}(5) \supset \mathrm{O}(3)\,, \tag{1}$$

$$\mathrm{U}(6) \supset \mathrm{SU}(3) \supset \mathrm{O}(3)\,, \tag{2}$$

$$\mathrm{U}(6) \supset \mathrm{O}(6) \supset \mathrm{O}(5) \supset \mathrm{O}(3)\,. \tag{3}$$

The dynamical symmetries associated with the above three chains correspond to three typical nuclear shapes or collective modes. These are the spherical vibration in the U(5) limit, the prolate rotational motion in the SU(3) limit, and γ-unstable motion in the O(6) limit. In addition, there also exist two "hidden" dynamical symmetries [30, 31] described by the following chains of U(6):

$$\mathrm{U}(6) \supset \overline{\mathrm{SU}(3)} \supset \mathrm{O}(3)\,, \tag{4}$$

$$\mathrm{U}(6) \supset \overline{\mathrm{O}(6)} \supset \mathrm{O}(5) \supset \mathrm{O}(3)\,, \tag{5}$$

in which generators of the $\overline{\mathrm{SU}(3)}$ and $\overline{\mathrm{O}(6)}$ dynamical symmetry groups can be constructed from the traditional SU(3) and O(6) group via the gauge transformation $s^\dagger \mapsto e^{i\phi}s^\dagger$ with $\phi = \pi$, and $\phi = \pm\frac{\pi}{2}$, respectively [30, 31, 44, 45]. The dynamical symmetry limits of the IBM are be described by Hamiltonians constructed out of group invariants (Casimir operators) in the corresponding group chains. As a result, the model in these three limits is exactly solvable. In this article, we only consider only the (2) and (4) limits, since they

correspond to the prolate and oblate shape phases, respectively, based on the original IBM considerations [6].

The eight generators of the SU(3) group can be expressed as

$$\hat{Q}_u = [s^\dagger \times \tilde{d} + d^\dagger \times \tilde{s}]^{(2)}_u - (\sqrt{7}/2)[d^\dagger \times \tilde{d}]^{(2)}_u \,, \tag{6}$$

$$\hat{L}_u = \sqrt{10}[d^\dagger \times \tilde{d}]^{(1)}_u \,, \tag{7}$$

by which the SU(3) invariant operators can be expressed as [34]

$$\hat{C}_2[\mathrm{SU(3)}] = 2\hat{Q}\cdot\hat{Q} + \frac{3}{4}\hat{L}\cdot\hat{L} \,, \tag{8}$$

$$\hat{C}_3[\mathrm{SU(3)}] = -\frac{4}{9}\sqrt{35}[\hat{Q}\times\hat{Q}\times\hat{Q}]^{(0)}_0 - \frac{\sqrt{15}}{2}[\hat{L}\times\hat{Q}\times\hat{L}]^{(0)}_0 \,. \tag{9}$$

For a given SU(3) irrep (λ,μ), the eigenvalues of the SU(3) invariant operators under the group chain $U(6) \supset SU(3) \supset O(3)$ are given as

$$\hat{C}_2[\mathrm{SU(3)}]\ |N(\lambda,\mu)KL> = (\lambda^2+\mu^2+\lambda\mu+3\lambda+3\mu)\ |N(\lambda,\mu)KL> \,, \tag{10}$$

$$\hat{C}_3[\mathrm{SU(3)}]\ |N(\lambda,\mu)KL> = \frac{1}{9}(\lambda-\mu)(2\lambda+\mu+3)(\lambda+2\mu+3)\ |N(\lambda,\mu)KL> \,, \tag{11}$$

where $|N(\lambda,\mu)KL>$ are basis vectors of the $U(6) \supset SU(3) \supset O(3)$ chain, where the additional quantum number K is that of the projection of the angular momentum on the third intrinsic axis [46]. The values of (λ,μ) contained in a symmetric representation $[N]$ of U(6) are given by [5]

$$\begin{aligned}
(\lambda,\mu) = \quad & (2N,0)\oplus(2N-4,2)\oplus(2N-8,4)\oplus ...\oplus(2,N-1) \text{ or } (0,N) \\
& \oplus(2N-6,0)\oplus(2N-10,2)\oplus(2N-14,4)\oplus ...\oplus(2,N-4) \text{ or } (0,N-3) \\
& \oplus(2N-12,0)\oplus(2N-16,2)\oplus(2N-20,4)\oplus ...\oplus(2,N-7) \text{ or } (0,N-6) \\
& \cdots \\
& \oplus(4,0)\oplus(0,2) \text{ for } N(\mathrm{mod3}) = 2 \\
& \oplus(2,0) \text{ for } N(\mathrm{mod3}) = 1 \\
& \oplus(0,0) \text{ for } N(\mathrm{mod3}) = 0 \,.
\end{aligned} \tag{12}$$

The angular momentum quantum number L contained in each representation (λ,μ) of SU(3) can be obtained according to the rules:

$$\begin{aligned}
& K = 0,\ 2, ...,\ \min\{\lambda,\mu\}; \\
& L = 0,\ 2, ...,\ \max\{\lambda,\mu\} \text{ for } K = 0 \,, \\
& L = K,\ K+1,\ K+2,\ \max\{\lambda,\mu\} \text{ for } K \neq 0 \,.
\end{aligned} \tag{13}$$

It should be noted that the basis vectors $|N(\lambda,\mu)KL>$ are not orthogonal with respect to K [46]. Therefore, an orthogonalization process of $|N(\lambda,\mu)KL>$ is needed in order to obtain the matrix element of each operator in the corresponding orthogonal basis [47], which can be realized with the algorithm shown in [48–50]. The orthogonalized $SU(3) \supset O(3)$ basis is often referred to as the Draayer-Akiyama basis.

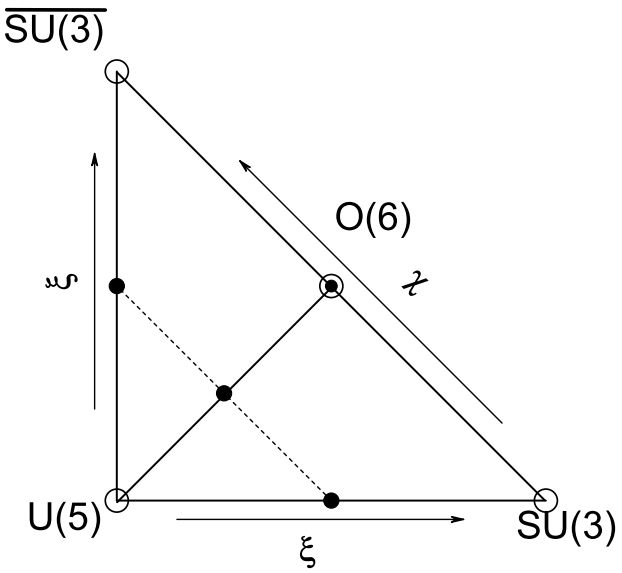

FIG. 1: The extended Casten triangle described by the Hamiltonian (14), where the central dot represent the critical point of the second-order phase transition along the U(5)-O(6) side, while the dash line and the line connecting the central dot with the O(6) point represent the first order phase transitions line of the transitions along the ξ and χ directions respectively.

We briefly recall the original prolate-oblate shape phase transitional description in the IBM. A typical consistent-Q formalism Hamiltonian [16] used to study the shape phase transition in the IBM can be written as

$$\hat{H}(\chi,\xi) = \varepsilon[(1-\xi)\hat{n}_d - \frac{\xi}{4N}\hat{Q}^{\chi}\cdot\hat{Q}^{\chi}]\,, \tag{14}$$

where ε is a scale parameter taken as 1 in the following, $\hat{n}_d = \sum_u d_u^\dagger d_u$ is the number operator of d-bosons, and

$$\hat{Q}^{\chi}_{\mu} = [s^\dagger \times \tilde{d} + d^\dagger \times \tilde{s}]^{(2)}_u + \chi[d^\dagger \times \tilde{d}]^{(2)}_u \tag{15}$$

with $-\sqrt{7}/2 \leq \chi \leq \sqrt{7}/2$ is the quadrupole operator. (14) can also be written as [51]

$$\begin{aligned}\hat{H}(\chi,\xi) &= [(1-\xi) - \frac{\xi\chi}{14N}(\chi+\frac{\sqrt{7}}{2})]\hat{C}_1[\mathrm{U}(5)] - \frac{\xi\chi}{14N}(\chi+\frac{\sqrt{7}}{2})\hat{C}_2[\mathrm{U}(5)] \\ &+\frac{\xi}{4N}(1+\frac{3}{\sqrt{7}}\chi+\frac{2}{7}\chi^2)\hat{C}_2[\mathrm{O}(5)] - \frac{\xi\chi}{56N}(\chi+2\sqrt{7})\hat{C}_2[\mathrm{O}(3)] \\ &+\frac{\xi\chi}{4\sqrt{7}N}\hat{C}_2[\mathrm{SU}(3)] - \frac{\xi}{4N}(1+\frac{2}{\sqrt{7}}\chi)\hat{C}_2[\mathrm{O}(6)]\,, \end{aligned} \tag{16}$$

where $C_k[\mathrm{G}]$ denotes the rank-k Casimir operator of group G. It is evident that (16) is just the Hamiltonian in the U(5) limit when $\xi = 0$; it is in the SU(3) limit when $\xi = 1$ and $\chi = -\sqrt{7}/2$; it is in the O(6) limit when $\xi = 1$ and $\chi = 0$; and it corresponds to the one in the $\overline{\mathrm{SU(3)}}$ symmetry [30] when $\xi = 1$ and $\chi = \sqrt{7}/2$. The whole parameter range of the model Hamiltonian (14) may be described by the extended Casten triangle [6], which is shown in Fig. 1. One can easily find various phase transition processes and related critical points from the triangle. Typically, there are second-order phase transition occurring along the U(5)-O(6) side, first-order phase transitions between the U(5) limit and points along the SU(3)-$\overline{\mathrm{SU(3)}}$ leg of the triangle, except for the O(6) limit point, and first-order phase transitions along the SU(3)-O(6)-$\overline{\mathrm{SU(3)}}$ line, in which the O(6) limit point is the corresponding critical point. Besides the three legs of the triangle, the first-order phase transitions generally occur inside of the triangle with the dash line and the line connecting the central dot with the O(6) point representing the collections of all the critical points of the first-order phase transition as seen in Fig. 1.

As mentioned above, the three-body interaction $[\hat{Q}'\times\hat{Q}'\times\hat{Q}']^{(0)}$ in the O(6) limit [33] can also generate rotational spectrum, which is completely different from that described by two-body interaction in the SU(3) limit. Similarly, a three-body interaction in the SU(3) limit, such as $[\hat{Q}\times\hat{Q}\times\hat{Q}]^{(0)}$ or $\hat{\mathrm{C}}_3[\mathrm{SU}(3)]$ defined in (9), can also bring out a novel rotational spectrum related with the oblate shape [34, 36, 39, 43]. We prefer to use the $\hat{\mathrm{C}}_3[\mathrm{SU}(3)]$ operator to construct a model Hamiltonian to describe oblate spectra.

The most general Hamiltonian up to including three-body terms with the SU(3) dynamical symmetry may be written as [41, 42]

$$\hat{H} = a_2\hat{C}_2[\mathrm{SU}(3)] + a_3\hat{C}_3[\mathrm{SU}(3)] + \delta\Omega + \eta'\hat{L}\cdot\hat{L}, \tag{17}$$

where $\Omega = [\hat{L}\times\hat{Q}\times\hat{L}]_0^{(0)}$ and a_2, a_3, δ and η' are adjustable parameters. Since the Ω term does not affect the nature of the shape phase transition in the ground state, for simplicity, we

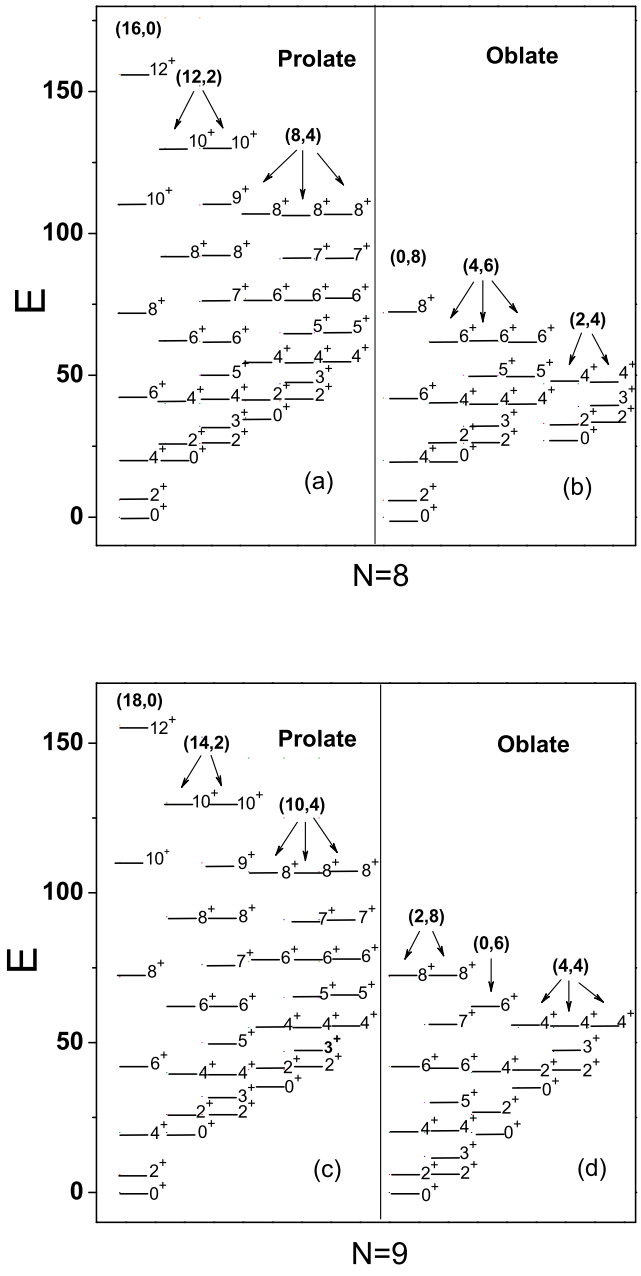

FIG. 2: The schematic spectra generated by the Hamiltonian (18) with $x = 0$ representing the prolate phase and $x = 1$ representing the oblate phase for $N = 8$ and 9, where the values of the second 0^+ energy levels in all the cases are set to 20 (arbitrary unit) by adjusting the scale parameter c, and η is taken as $\frac{1}{c}$.

take $\delta = 0$ in (17) and rescale the other parameters in order to investigate the prolate-oblate shape phase transition. Then, the Hamiltonian may be rewritten as

$$\hat{H} = c[\frac{(x-1)}{N}\hat{C}_2[\mathrm{SU}(3)] + \frac{x}{N^2}\hat{C}_3[\mathrm{SU}(3)] + \eta\hat{L}\cdot\hat{L}], \tag{18}$$

in which $c = N(a_3N - a_2)$, $x = a_3N(a_3N - a_2)$, and $\eta = \eta'/c$ in comparison to the parameterization shown in (24). In (18), the $\hat{L}\cdot\hat{L}$ term is used to avoid level degeneracy for levels with different L. Further, (18) can be used either to describe spectra if $x = 0$ is taken, or to describe that with an oblate shape if $x = 1$ is taken. Thus, one can realize a prolate-oblate phase transition by varying $x \in [0, 1]$. Owning to the exact SU(3) symmetry, (18) can be analytically solved for any values of the parameters and boson number N. This situation is different from the common quantum phase transition studied with a Hamiltonian [26, 28]

$$\hat{H} = (1-x)\hat{H}_1 + x\hat{H}_2\,, \tag{19}$$

where $\hat{H}_1$ and $\hat{H}_2$ describe two different phases respectively. In general $\hat{H}_1$ and $\hat{H}_2$ are mutually incompatible, $[\hat{H}_1, \hat{H}_2] \neq 0$, having no common eigenstate. On the other hand, $\hat{C}_2[\mathrm{SU}(3)]$ and $\hat{C}_3[\mathrm{SU}(3)]$ in (18) do commute with each other and therefore have common eigenstates, which are the basis vectors of the group chain (2). In other words, the different phases are usually described by the terms in the Hamiltonian with different symmetries, while the prolate and oblate phases in this case are described within the same SU(3) limit. Though the two phases are described within the same SU(3) limit, the low-lying structures and the corresponding eigenstates obtained with only the $\hat{C}_2[\mathrm{SU}(3)]$ in the Hamiltonian and those with only the $\hat{C}_3[\mathrm{SU}(3)$ term are completely different since they are related to different SU(3) irreps. Thus the case considered here is an asymmetric prolate-oblate shape phase transition in contrast to the former SU(3)-O(6)-$\overline{\mathrm{SU}(3)}$ case studied in [6].

Specifically, the typical lowing-lying spectrum with the prolate shape and those with oblate shape in our scheme are illustrated in Fig. 2, where the results calculated with (18) are shown for $N = 8$ and $N = 9$ representing the $N =$ even and $N =$ odd cases respectively. As seen from the panel (a) of Fig. 2, the ground band in the prolate case belongs to the SU(3) irrep $(2N, 0)$, from which $L_{\max} = 2N$. Moreover, the irrep $(2N-4, 2)$ in the prolate phase includes the two lowest excited rotational bands corresponding to the β- and γ- bands, in which the energy levels with the same L value are degenerate. As for the oblate spectrum for $N =$ even shown in the panel (b) of Fig. 2, the ground band belongs to the SU(3)

irrep $(0, N)$ with $L_{\max} = N$, and the β-, γ-, and the lowest $K = 4$ bands are all belong to the irrep $(4, N-2)$, where the energy levels are also degenerate for the same L. In addition, the prolate spectrum for $N =$ odd is similar to that for $N =$ even as shown in the panels (a) and (c) of Fig. 2. But there are some notable differences in the oblate case. For example, both the ground band and the γ-band belong to the irrep $(2, N-1)$ seen from the panel (d) of Fig. 2. As a result, an obvious feature of the oblate spectrum for $N =$ odd is that eigenenergies of the double-degenerate levels, such as 2^+, 4^+ and 6^+ etc, increase with increasing of L; and E2 transitions between the ground band and the γ-band are much stronger than those between the β-band and the ground band or the γ-band since inter-band transitions within the same $SU(3)$ irrep are much stronger [5]. These features may be used to distinguish oblate from prolate shapes. Moreover, the third order term $\hat{C}_3[\mathrm{SU(3)}]$ is used to describe pure rotational motion for oblate case similar to the $\overline{\mathrm{SU(3)}}$ description. Actually, spectra generated by the $\overline{\mathrm{SU(3)}}$ and the SU(3) invariants up to two-body terms are exactly symmetric [6, 25], namely the prolate spectrum generated by the $\hat{C}_2[\mathrm{SU(3)}]$ are the same as the oblate spectrum generated by the $\hat{C}_2[\overline{\mathrm{SU(3)}}]$. As a result, what have been shown in Fig. 2 can also be regarded as comparisons between oblate spectra generated by the $\overline{\mathrm{SU(3)}}$ invariant and those generated by the third order invariant $\hat{C}_3[\mathrm{SU(3)}]$ within the SU(3) limit. However, as observed from experimental results, most oblate nuclei with positive quadrupole moments may involve other collective motions, such as γ-unstable motion described by the O(6) symmetry, which may distort rotational features described by the third order term $\hat{C}_3[\mathrm{SU(3)}]$.

III. PROLATE-OBLATE SHAPE PHASE TRANSITION IN THE LARGE-N LIMIT

To investigate the prolate-oblate shape phase transition in the large-N limit, the coherent state (also called the intrinsic state) defined as [5, 43]

$$|\beta, \gamma, N> = \frac{1}{\sqrt{N!(1+\beta^2)^N}}[s^\dagger + \beta\cos\gamma d_0^\dagger + \frac{1}{\sqrt{2}}\beta\sin\gamma(d_2^\dagger + d_{-2}^\dagger)]^N|0> \tag{20}$$

may be adopted to study the classical limit of the model. Ground state energy corresponding to the Hamiltonian (18) in the large-N limit is then estimated by the expectation value in the coherent state, $<\beta, \gamma, N|\hat{H}|\beta, \gamma, N>$. Thus, the ground state energy per boson in the

large-N limit can be expressed as

$$E(x,\beta,\gamma) = -(1-x)\frac{\beta^2}{(1+\beta^2)^2}[\beta^2+4\sqrt{2}\beta\cos3\gamma+8] \tag{21}$$
$$-x\frac{16}{441}\sqrt{7}\frac{\beta^3}{(1+\beta^2)^3}[-\frac{7}{8}\sqrt{7}\beta^3(2\cos^2 3\gamma-1)-\sqrt{14}(\frac{21}{4}\beta^2+14)\cos3\gamma-21\sqrt{7}\beta]\,,$$

where $c=1$ is taken in (18). In order to show the phase structure and the transition, contour diagrams of the ground state energy per boson at several values of the control parameter x are shown in Fig. 3. As clearly shown in Fig. 3, for $x<0.6$, there is a global minimum around $\beta=1.4$ and $\gamma=0^\circ$ that represents a prolate phase. With increasing x, an oblate minimum begins to emerge around $\beta=0.7$ and $\gamma=60^\circ$. At $x=0.6$, the oblate minimum is connected with the prolate minimum and develops into a minimal region, in which a prolate-oblate shape phase transition occurs. When $x>0.6$, the minimal region becomes a global minimum point around $\beta=0.7$ and $\gamma=60^\circ$ indicating that an oblate phase appears. As shown in Fig. 3, γ varies from 0° and 60° in the equilibrium valley at the critical point around $x=0.6$, which indicates a γ-soft shape. As a result, there is no stable triaxial shape occurring at the critical point of the prolate-oblate shape phase transition in this description. Actually, the shape at the critical point appears similar to that found in the O(6) limit. But the difference between the case at this critical point and that in the O(6) limit is also evident. For example, at the critical point, the β variable in the equilibrium valley can be taken from 0.7 to infinity, while the β variable in the equilibrium positions in the O(6) limit can only be taken as two fixed values.

Furthermore, the ground state energy per boson $E_{\rm g}$ and the β and γ values at the corresponding equilibrium point are calculated in order to clarify the order of the shape phase transition. The results are shown as functions of the control parameter x in Fig. 4. It is clear from these results that the ground state energy per boson $E_{\rm g}$ varies with x around the critical point; specifically, $E_{\rm g}=-4+\frac{52}{9}x$ for $x<0.6$, and $E_{\rm g}=-1+\frac{7}{9}x$ for $x>0.6$. As a result, the first derivative $\frac{\partial E_{\rm g}(x)}{\partial x}$ is discontinuous at $x=0.6$, which indicates that the prolate-oblate shape phase transition is of first order. In addition, the equilibrium values of β and γ are constants with $\beta=\sqrt{2}$ and $\gamma=0^\circ$ for the prolate phase when $x<0.6$, while $\beta=\sqrt{2}/2$ and $\gamma=60^\circ$ for the oblate phase when $x>0.6$, which confirms the first-order phase transition occurring at the critical point $x=0.6$. It should be noted that the same phase diagram in the classical limit based on a similar Hamiltonian was also obtained and discussed in [43]. In the large-N limit, since the $\hat{L}^2$ and $[\hat{L}\times\hat{Q}\times\hat{L}]^{(0)}$ terms contribute

nothing to the potential surface, the Hamiltonian (18) will be equivalent to the one used in [43] if setting the parameters $2c(1-x)=1$, $\xi=0$, $\chi=-\sqrt{7}/2$ and $k_3=\frac{2\sqrt{35}x}{9(1-x)}$, where ξ, χ and k_3 are the parameters of the Hamiltonian used in [43]. As a result, the potential structure generated by the Hamiltonian (18) should be the same as that given in [43] within the above parameter restrictions.

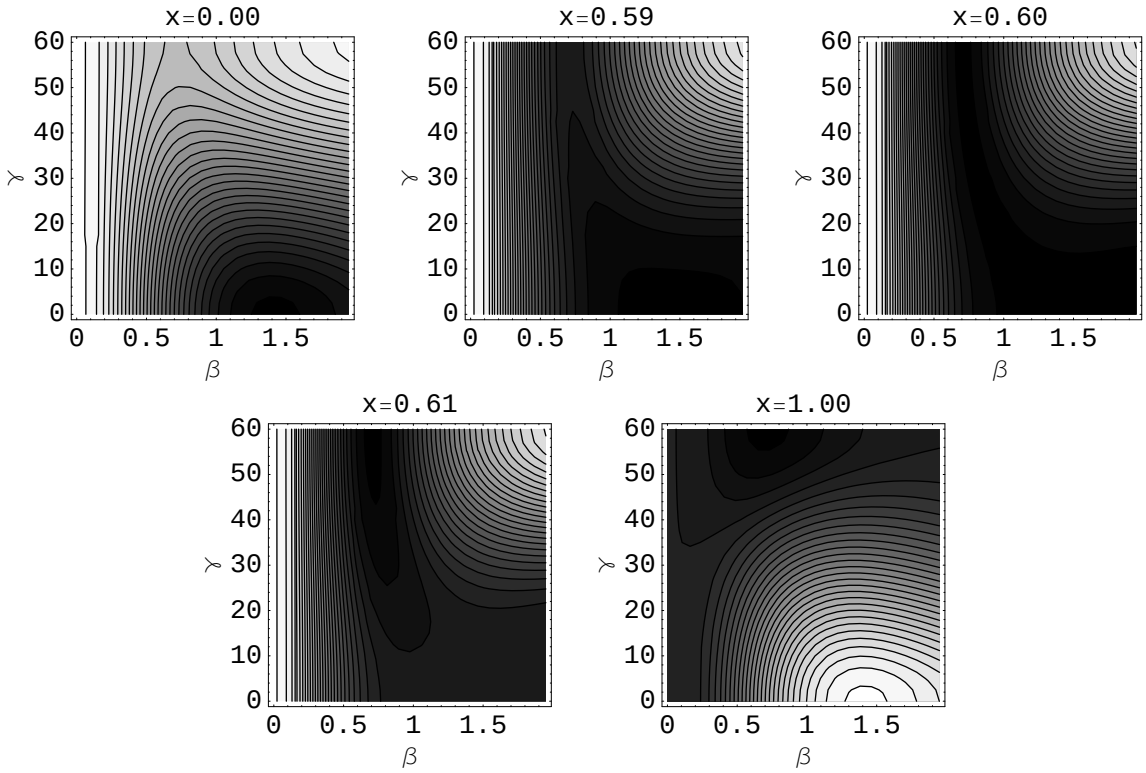

FIG. 3: The contour diagrams of the ground state energy per boson with $x=0.00, 0.59, 0.60, 0.61$ and 1.00 shown in the sub-diagrams in the order from left to right and from top to bottom, in which the unit of the γ variable is degree. In addition, the smaller the energy, the darker the color.

IV. PROLATE-OBLATE SHAPE PHASE TRANSITION IN FINITE SYSTEMS

The analysis shown in the previous section indicates that a first-order shape phase transition in the large-N limit is induced by the three-body interaction with SU(3) symmetry. However, the boson number N is always finite in realistic systems. As a result, it is important to investigate the finite-N effects on the phase transition [6]. Most studies about the finite-N effects in phase transitions can only be carried out numerically since the problem cannot

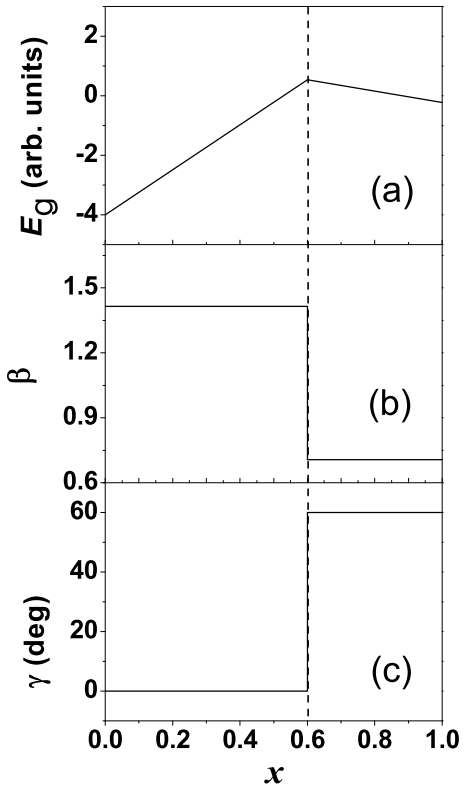

FIG. 4: (a) The ground state energy per boson $E_{\rm g}$; (b) the corresponding equilibrium values of β; (c) the corresponding equilibrium values of γ. All the quantities are shown as functions of the control parameter x.

be solved analytically in most cases. However, The Hamiltonian (18), which preserves the exact SU(3) symmetry, is analytically solvable. Therefore, it provides a situation in the IBM to analytically study the whole process in the prolate-oblate shape phase transition for any number of bosons.

In order to define the shape of the system for finite-N cases, we resort to the relations between the shape variables $(\beta,\ \gamma)$ of the collective model and the $(\lambda,\ \mu)$ values of the SU(3) irrep [39], from which we have

$$\begin{aligned} \kappa\beta\cos\gamma &= \frac{1}{3}(2\lambda+\mu+3), \\ \kappa\beta\sin\gamma &= \frac{1}{\sqrt{3}}(\mu+1) \end{aligned} \tag{22}$$

with

$$\kappa = \sqrt{\frac{5}{9\pi}} A r_0^2\,, \tag{23}$$

where A denotes the number of like particles and r_0^2 is a dimensionless mean square radius [39]. In the following, κ is treated as a parameter to be determined in the IBM. Accordingly, one can write the shape variables β and γ as the functions of the quantum number λ and μ with

$$\beta = \frac{2}{3\kappa}\sqrt{\lambda^2+\mu^2+\lambda\mu+3\lambda+3\mu+3},$$
$$\gamma = \tan^{-1}(\frac{\sqrt{3}(\mu+1)}{2\lambda+\mu+3}). \tag{24}$$

As discussed in Sec. II, the ground state in the prolate phase belongs to the SU(3) irrep $(2N,0)$, while the one in the oblate phase corresponds to the SU(3) irrep $(0,N)$ for $N=$ even or $(2,N-1)$ for $N=$ odd. According to (24), one gets $\gamma_{\rm P}=\tan^{-1}(\frac{\sqrt{3}}{4N+3})$ for the ground state in the prolate phase, and $\gamma_{\rm O}=\tan^{-1}(\frac{\sqrt{3}(N+1)}{N+3})$ for $N=$ even or $\gamma_{\rm O}=\tan^{-1}(\frac{\sqrt{3}N}{N+2})$ for $N=$ odd for the ground state in the oblate phase. It is clear that $\gamma_{\rm P}=0^\circ$ and $\gamma_{\rm O}=60^\circ$ are given for the prolate phase and the oblate phase, respectively, when $N\to\infty$. The results are consistent with those obtained from the coherent theory discussed in Sec. III, where the equilibrium β and γ values just correspond to the β and γ values for the ground state. As for the shape variable β in the ground state, one get

$$\beta_{\rm P} = \frac{4}{3\kappa}\sqrt{N^2+\frac{3}{2}N+\frac{3}{4}} \tag{25}$$

in the prolate case, and

$$\beta_{\rm O} = \frac{2}{3\kappa}\sqrt{N^2+3N+3} \quad (\text{for } N=\text{even}) \tag{26}$$

or

$$\beta_{\rm O} = \frac{2}{3\kappa}\sqrt{N^2+3N+9} \quad (\text{for } N=\text{odd}) \tag{27}$$

in the oblate case. It is easy to see that $\beta_{\rm P}/\beta_{\rm O}=2$ in the large-N limit. It is very interesting to observe that the result also agrees with that calculated from the coherent theory, by which one can get the equilibrium β value as $\beta_{\rm P}=\sqrt{2}$ for the prolate phase and $\beta_{\rm O}=\sqrt{2}/2$ for the oblate phase in the large-N limit as shown in Fig. 4. Thus, we have $\beta_{\rm P}/\beta_{\rm O}=2$. We conclude that the shape variables β and γ defined in (22) and those defined in the coherent theory are consistent with each other not only in quality but also in quantity in the large-N limit. Moreover, one can extract κ by assuming $\beta_{\rm P}|_{N\to\infty}=\sqrt{2}$ in (25) and $\beta_{\rm O}|_{N\to\infty}=\sqrt{2}/2$ in (26) or (27). Concretely, one can get $\kappa^2=\frac{8}{9}N^2$ in the leading order. Inputting κ^2 into

TABLE I: Excited energies corresponding to all irreps (λ, μ) of SU(3) for $N = 12$ for some values of x with $0.00 \leq x \leq 1.00$. The results are obtained by solving the eigen-equation of the Hamiltonian (18) with $c = 1$ and $\eta = 0$.

x	(λ, μ)																		
	(24,0)	(20,2)	(16,4)	(12,6)	(8,8)	(4,10)	(0,12)	(18,0)	(14,2)	(10,4)	(6,6)	(2,8)	(12,0)	(8,2)	(4,4)	(0,6)	(6,0)	(2,2)	(0,0)
0.00	-54.00	-42.50	-33.00	-25.50	-20.00	-16.50	-15.00	-31.50	-23.00	-16.50	-12.00	-9.50	-15.00	-9.50	-6.00	-4.50	-4.50	2.00	0.00
0.30	-30.15	-24.69	-20.17	-16.61	-14.00	-12.34	-11.61	-18.64	-14.18	-1076	-8.40	-7.09	-9.38	-6.21	-4.20	-3.34	-2.96	-1.40	0.00
0.57	-8.57	-8.57	-8.57	-8.57	-8.57	-8.57	-8.57	-7.00	-6.19	-5.57	-5.14	-4.90	-4.28	-3.24	-2.57	-2.29	-1.57	-0.86	0.00
0.63	-3.80	-5.00	-6.00	-6.79	-7.37	-7.74	-7.90	-4.42	-4.42	-4.42	-4.42	-4.42	-3.16	-2.58	-2.21	-2.05	-1.26	-0.74	0.00
0.70	1.65	-0.64	-3.08	-4.76	-6.00	-6.79	-7.13	-1.49	-2.41	-3.11	-3.60	-3.87	-1.88	-1.83	-1.80	-1.79	-0.91	-0.60	0.00
1.00	25.50	16.88	9.75	4.13	0.00	-2.63	-3.75	11.38	6.42	2.63	0.00	-1.46	3.75	1.46	0.00	-0.63	0.63	0.00	0.00

(24), one gets $\beta_{\rm P} = \sqrt{2}$ and $\beta_{\rm O} = \sqrt{2}/2$ in the large-N limit. The results are the same as those obtained in the coherent state theory.

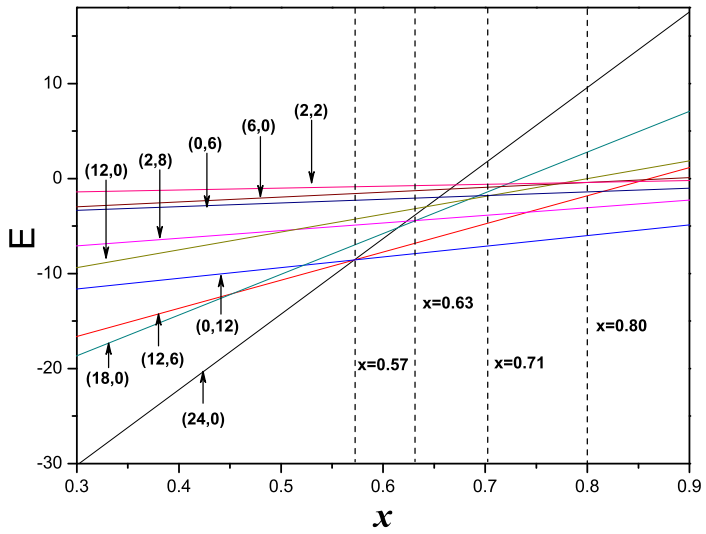

FIG. 5: (Color online) Several excited energy levels with specific (λ, μ) which cross with each other at the critical-like points with variation of the control parameter x. The relevant parameters are taken as the same as those used in Table. I

To investigate how the system evolves from the prolate to the oblate phase, eigenenergies

calculated from the Hamiltonian (18) are listed in Table. I, where eigenenergies corresponding to all the SU(3) irreps (λ, μ) for $N = 12$ are shown for several values of the control parameter x. It can be clearly seen from Table. I that the ground state always corresponds to the symmetric $(24, 0)$ irrep of $SU(3)$ when $x < 0.57$, and corresponds to $(0, 12)$ irrep when $x > 0.57$. The results indicate that the point $x = 0.57$ is just the critical point, at which the levels corresponding to the irreps (λ, μ) with $\lambda + 2\mu = 24$ become the same lowest energy levels. In other words, the ground state is degenerate with the quantum numbers (λ, μ) satisfying $\lambda + 2\mu = 24$ at the critical point of phase transition. As can be seen from the model Hamiltonian (18), the combination of the second and the third order Casimir operators will result in level-crossing when the control parameter x satisfies certain conditions, at which the first order quantum phase transition takes place. And indeed, such situations also occur in excited levels. For example, when $x = 0.63$, the excited energy levels corresponding to the SU(3) irreps (λ, μ) with $\lambda + 2\mu = 18$ become degenerate as shown in Table. I. Actually, there are several level-crossing points, such as those with $x = 0.63$, 0.71, and 0.80, etc. as shown in Fig. 5, where the excited energy levels with (λ, μ) satisfying $\lambda + 2\mu = 2N - b$ are degenerate for a fixed value of b with $b = 6,\ 12,\ 18$, etc. As shown in Fig. 5, these are just the level-crossing points of levels labeled with $(2N - b, 0)$ and those labeled with $(0, N - \frac{b}{2})$ with $\frac{b}{2} =$ even or those labeled with $(2, N - \frac{b}{2} - 1)$ with $\frac{b}{2} =$ odd. As the analysis presented in [9], the energy level-crossing resulting in a first-order quantum phase transition in the finite-N system also occurs in the SU(3)-O(6)-$\overline{\text{SU(3)}}$ phase transitional description, where one of the level-crossing points coincides with the O(6) limit point. Actually, the level-crossing point in our model also coincides with the critical point $x_c = 0.6$ in the large-N limit because the value of the level-crossing point varies as $x = \frac{3N}{5N-b+3}$ with $b = 6, 12, 18, ...$ for a fixed boson number N. As mentioned above, the energy levels corresponding to the irreps (λ, μ) satisfying $\lambda + 2\mu = 2N - b$ are degenerate at the level-crossing points. As a result, one can get several sets of levels with the same eigenenergy at the level-crossing points x_c as a function of b in the large-N limit. If the energy of the ground level with 0_1^+ and $b = 0$ is set to 0, and all excited levels are normalized to the 0_2^+ level with $b = 6$, one get energy ratios $E_{0_3^+}/E_{0_2^+} = 2$ and $E_{0_4^+}/E_{0_2^+} = 3$. Generally, we have $E_{0_n^+}/E_{0_2^+} = n - 1$ with $n = \frac{6+b}{6}$, where $E_{0_n^+}$ are levels with $b = 6(n - 1)$. Therefore, these degenerate 0^+ levels generate a harmonic spectrum [52, 53]. In addition, the first order quantum phase transition also occurs in excited part of the spectrum [54, 55], of which possible effects will be further discussed

elsewhere.

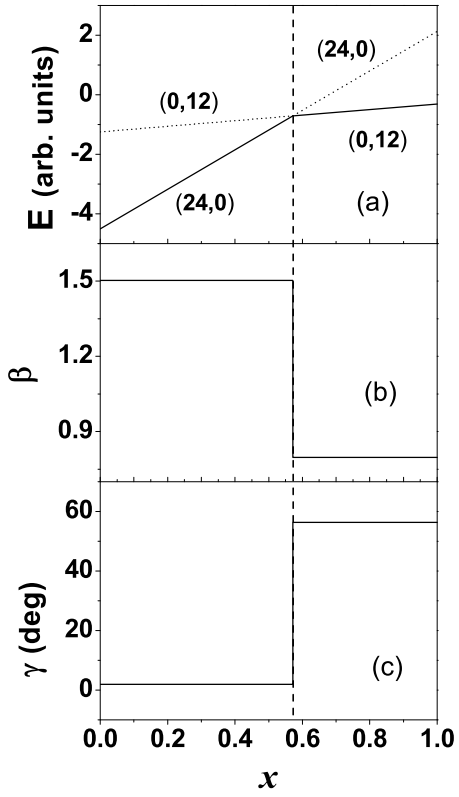

FIG. 6: (a) The ground state energy per boson; (b) the corresponding β value; (c) the corresponding γ value. All the quantities are give as functions of the control parameter x for a $N = 12$ boson system. The relevant parameters are taken the same as those used in Table. I

To explore the role finite N effects have on the shape phase transition, and to compare this with the large-N limit, the ground state energy per boson, along with the corresponding β and γ values, were calculated as functions of x. The results are shown in Fig. 6. From this one can see that the ground level belongs to the $(24, 0)$ irrep when $x < 0.57$ and transitions over to the $(0, 12)$ irrep for larger x values, displaying upon crossing into the $x > 0.57$ range a different dependence on x. It is obvious that the first-order derivative of the ground state energy $\frac{\partial E_{\rm g}(x)}{\partial x}$ is discontinuous at $x_{\rm c} = 0.57$, which indicates a first order prolate-oblate phase transition occurring at the critical point $x_{\rm c} = 0.57$ for the $N = 12$ boson system. Moreover, $\frac{\partial \beta}{\partial x}$ and $\frac{\partial \gamma}{\partial x}$ in the ground state are also discontinuous at the critical point, which further confirms that a first order prolate-oblate phase transition occurs in the model system. In comparison to the large-N limit, one finds that the finite-N effects changes the position of

the critical point, but not by much, $x_c = 0.57$ compared to $x_c = 0.60$ in the large-N limit.

From the explicit expression for the eigenvalues of (18) for fixed boson number N, one can show that the ground state energy per boson in the prolate phase can be expressed in terms of the control parameter x as

$$E_g = -4 + \frac{52}{9}x + \frac{10}{N}x + \frac{2}{N^2}x - \frac{6}{N}\,, \tag{28}$$

and the corresponding one in the oblate phase is

$$E_g = -1 + \frac{7}{9}x + \frac{2}{N}x + \frac{1}{N^2}x - \frac{3}{N}\,. \tag{29}$$

In the large-N limit, the results of (28) and (29) will become the corresponding results calculated from the coherent state theory shown in Sec. III. Since the ground state energy in the prolate phase is equal to the one in the oblate phase at the critical point x_c, one obtains $x_c = \frac{3N}{3+5N}$, which just equals to $x_c = 0.6$ in the large N limit, and is consistent with the result obtained from the coherent state theory. We conclude that, in this case, the results derived from finite-N system in the large-N limit are completely consistent with those obtained from the coherent state theory. Moreover, the prolate-oblate shape phase transition is well defined in this finite boson system and is due to the level-crossing according to the above discussion.

V. EFFECTIVE ORDER PARAMETERS FOR PHASE TRANSITIONS

Although the shape variables β and γ can be taken as classical order parameters to identify the shape phase transition, they cannot be directly measured in experiment. Therefore, the quadrupole invariants q_2 and K_3 (renormalized q_3) [6, 56] defined by

$$q_2 = \quad t^2 < 0_1^+|\hat{Q}\cdot\hat{Q}|0_1^+>\,, \tag{30}$$

$$q_3 = \quad \sqrt{\frac{35}{2}}t^3 < 0_1^+|[\hat{Q}\times\hat{Q}\times\hat{Q}]^{(0)}|0_1^+>\,, \tag{31}$$

$$K_3 = \quad \frac{q_3}{{q_2}^{3/2}}\,, \tag{32}$$

where t is the effective charge, were calculated. The results as functions of x are shown in Fig. 7.

These quantities can be used to define effective order parameters to identify the shape phases and their transition in experiment. In addition, the spectroscopic quadrupole moment $Q(2_1^+)$ of the first 2^+ state is also taken as an effective order parameter to measure the

prolate-oblate shape phase transition. $Q(2_1^+) < 0$ indicates a prolate phase and $Q(2_1^+) > 0$ represents an oblate phase. Another quantity β_2 related to the quadrupole deformation but different from the β variable is also considered, which is defined as [25, 57, 58]

$$\beta_2 = -\text{sign}(\hat{Q}(2_1^+))\frac{4\pi}{3ZR_0^2}[\frac{B(E2;0_g^+ \to 2_1^+)}{e^2}]^{1/2}\,, \tag{33}$$

where $\text{sign}(\hat{Q}(2_1^+))$ is the sign of the quadrupole moment of the first 2^+ state, Z is the proton number, R_0 is the mean radius of nucleus, and e is the charge. Accordingly, the $E2$ operator is simply chosen as $T(E2) = t\hat{Q}$ to calculate the $B(E2;0_g^+ \to 2_1^+)$. The calculated results for $Q(2_1^+)$ and those for β_2 are both shown in Fig. 8.

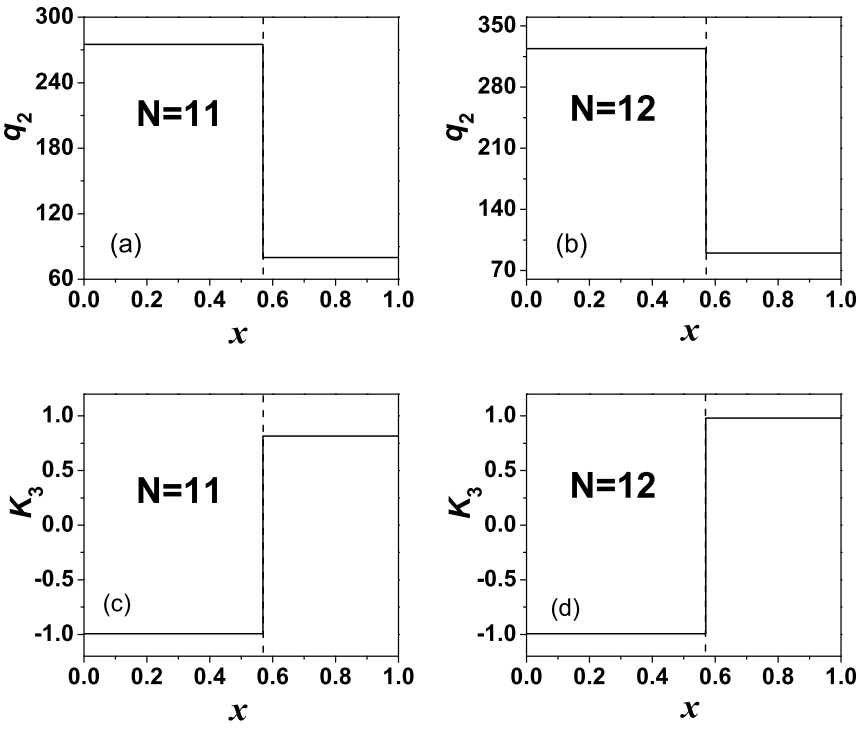

FIG. 7: The quadrupole invariants q_2 (in e^2b^2) and K_3 (normalized q_3) as functions of x in the ground state, where $t = 1$ eb was used and the other relevant parameters are taken to be the as same as those used in Table. I

It can be clearly seen in Fig. 7 that there is a sudden change in the value of all these quantities through the prolate-oblate phase transition. For example, $K_3 \simeq -1$ across the prolate phase but then suddenly jumps to $K_3 \simeq 1$ after the critical point, which is similar to the behavior seen for K_3 in the SU(3)-O(6)-$\overline{\text{SU(3)}}$ phase transitional description [6],

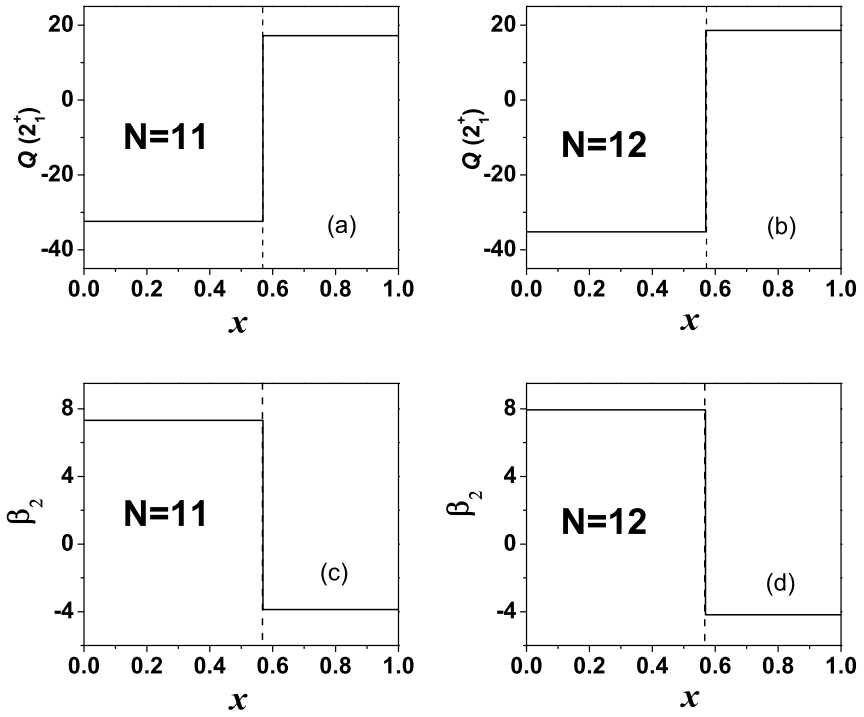

FIG. 8: The same as Fig. 7 but for the quadrupole $Q(2_1^+)$ (in eb) and the quadrupole deformation parameter β_2, where the effective charge $t = 1$ eb and a constant $4\pi/ZR_0^2 = 0.81$ b^{-1} were used. The other relevant parameters are taken the same as those used in Table. I.

except that the change of K_3 around the O(6) critical point is smoother than that shown in the panels (c) and (d) of Fig. 7. Also shown in the panels (a) and (b) of Fig. 7 is the order parameter q_2 (with the effective charge t set to unity) which shows a similar phase transitional behavior. Specifically, q_2 retains its large value, $q_2 = 2N^2 + 3N$, across the prolate phase, but then drops suddenly to $q_2 = (N^2 + 3N)/2$ beyond the critical point and holds at this lower value throughout the oblate phase; that is, through the prolate-oblate shape phase transition the amplitude of q_2 decreases by about 3/4. This behavior of q_2 stands in contrast with what happens in the SU(3)-O(6)-$\overline{\text{SU(3)}}$ phase transitional description [6] where the value of q_2 in the prolate phase equals that in the oblate phase.

As shown in Fig. 8, both $Q(2_1^+)$ and β_2 show a sign change in the transition from prolate to oblate shape, just as K_3 does. For example, $Q(2_1^+)$ takes a negative value in the prolate phase, and flips to a positive value in the oblate phase, a feature that may be the most direct signal indicating the phase transition from prolate to oblate shape in

experiment. But in contrast to K_3, $Q(2_1^+)$ also shows a asymmetric phase transitional feature similar to those given by q_2. The absolute value of $Q(2_1^+)$ in the prolate phase may be as twice that in the oblate phase, which indicates that the deformation of the oblate nuclei should be much smaller than that of prolate nuclei along the prolate-oblate shape phase transition. Accordingly, the absolute value of β_2 in the prolate phase is also much larger than in the oblate phase, which further confirms that the present SU(3) prolate-oblate phase transition pattern is an asymmetric one, in contrast to the SU(3)-O(6)-$\overline{\text{SU(3)}}$ phase transitional description. Furthermore, one can also measure ratios of the deformation quantities in the prolate phase and the oblate phase by defining $R_Q = |Q_{\rm P}(2_1^+)| \ / \ |Q_{\rm O}(2_1^+)|$ and $R_\beta = |\beta_{2\rm P}| \ / \ |\beta_{2\rm O}|$, where $|A_{\rm P}|$ ($|A_{\rm O}|$) is the absolute value of the quantity A in the prolate (oblate) phase. Our calculation shows that $R_Q \approx R_\beta \approx \sqrt{\frac{4N^2+3N}{N^2+3N}}$, which, to leading order, is in accordance to the ratio $\beta_{\rm P}/\beta_{\rm O}$ obtained from (25)-(27). Therefore, it seems that the observables $Q(2_1^+)$ and β_2 are qualified to measure the ground state deformation to see whether the nuclei is prolate or oblate instead of the deformation parameter β.

From an experimental perspective, W, Pt, and Os isotopes in A = 180 $\sim$ 200 mass region may be considered as candidates to show the prolate-oblate phase transition [7, 25, 59]. Since these even-even nuclei with $\Delta A = 2$ differ from each other by one boson and the properties of the low-lying states are experimentally known, in the following, ^{180}Hf [60], ^{182,184,186}W [61–63], ^{188,190}Os [64, 65], and ^{192,194,196,198}Pt [66–69] will be chosen to be fitted by the theory because there is an evident sign change in $Q(2_1^+)$ of ^{192}Pt indicating a prolate-oblate shape phase transition emerging with the variation of the mass number A. Specifically, experimental data of $Q(2_1^+)$ and β_2 together with the corresponding results calculated from the theory are shown in Fig. 9. Some low-lying energy levels calculated from the theory in comparison to the corresponding experimental results are shown in Fig. 10. As shown in Fig. 9, the experimental data are well reproduced by our model, and clearly indicates a definite prolate-oblate shape phase transition occurring at $A = 192$, where the $Q(2_1^+)$ value changes to be positive when $A > 192$ from negative when $A < 192$ seen from the panel (9a). Moreover, the asymmetric feature of the prolate-oblate phase transition are also shown from experimental results. We observe that the absolute value of $Q(2_1^+)$ and β_2 of the prolate nuclei are evidently larger than that of the oblate nuclei concerned. In addition, the absolute values of $Q(2_1^+)$ and β_2 in prolate or oblate nuclei decrease with the decreasing of the boson number. And indeed, this tendency shown from the experiment data is well reproduced by

the theoretical results shown in Fig. 9.

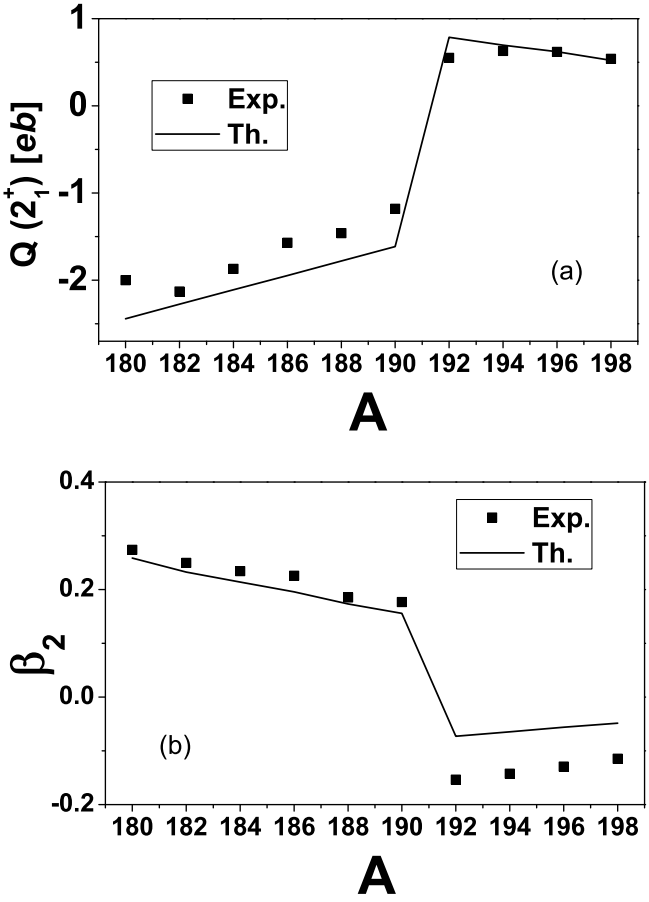

FIG. 9: Comparison of the theoretical values (solid line) obtained with Hamiltonian (18) and the corresponding experimental data of the quadrupole moment $Q(2_1^+)$ and the quadrupole deformation parameter β_2 for ^{180}Hf, ^{182,184,186}W, ^{188,190}Os, and ^{192,194,196,198}Pt. In our calculation, a constant effective charge with $t = 0.06$ eb was used and R_0 has been taken to be $1.2\mathrm{A}^{1/3}$fm [57] with A being the mass number.

It should be emphasized that the theoretical results with a fixed boson number N are not sensitive to the variation of the control parameter x in (18) except the case around the critical point with $x = x_c$, which indicates that the theoretical predictions given in Fig. 9 are almost parameter independent up to an overall scale factor. As shown In Fig. 10, the asymmetric feature is also noticeable in the low-lying energy levels. Concretely, one can clearly seen from Fig. 10 that the energy gaps between the level with L and that with $L-2$ observed in experiment show a sudden increase at $A = 192$, especially for $L = 2$ levels. This

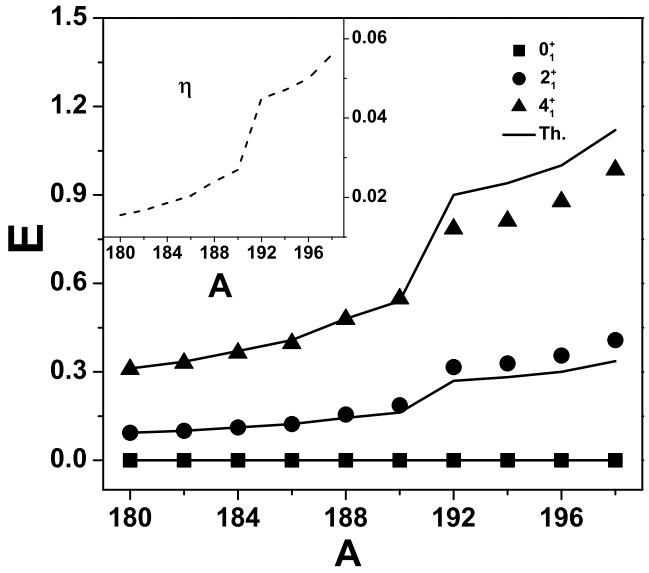

FIG. 10: The excited energy levels (in MeV) of the low-lying 0_1^+, 2_1^+ and 4_1^+ states for ^{180}Hf, ^{182,184,186}W, ^{188,190}Os, and ^{192,194,196,198}Pt. The experimental data are denoted by the symbols and the theoretical results represented by the solid lines are calculated with the Hamiltonian (18), where the parameter c has been taken as $c = 1$ and the values of the parameter η fitted by the experiments are shown in the insert.

indicates that the fitted η value increases rapidly around the point of $A = 192$ as shown in the insert of Fig. 10. On the other hand, by considering the moment of inertia defined in the triaxial rotor model [70, 71], namely $T_k = 4B\beta^2\sin^2(\gamma - \frac{2k}{3}\pi)$ with $k = 1,\ 2,\ 3$ and B being the mass parameter, one can find that the smaller the deformation parameter β, the smaller the two nonzero components of T_k for an axial deformed system represented by $\gamma = 0^\circ$ or $\gamma = 60^\circ$. As a result, a possible explanation in the triaxial rotor model for the spectral behavior around $A = 192$ in experiment shown in Fig. 10 is that the deformation of ^{192}Pt is much smaller than that of ^{190}Os. Since the deformation can be directly reflected from the quadrupole moment $Q(2_1^+)$ [70], the results shown in Fig. 9 indicate that the deformation of ^{192}Pt may be much smaller than that of ^{190}Os. Moreover, the analysis on energy surface given in [72–74] also indicate that the deformation of ^{192}Pt is indeed smaller than that of ^{190}Os. In short, the evolution of the low-lying spectrum shown in Fig. 10 further confirm

that the prolate-oblate shape phase transition occurring at $A = 192$ is asymmetric.

In addition, there are some quantitative deviations of our theoretical predictions from the corresponding experimental results, especially for the 4_1^+ level in the oblate nuclei. The deviations indicate that the excited states of these nuclei are not purely rotational. Some other collective modes may also be involved in the low-lying part of the spectra. The prolate-oblate shape phase transitional description within the SU(3) limit considered is a simplified model to manifest the asymmetric shape phase transition in this mass region. More complicated descriptions, such as mixed symmetry schemes beyond the SU(3) limit may also be needed to reproduce the experimental results of these nuclei better in quantity.

VI. SUMMARY AND CONCLUSIONS

In summary, we have analyzed a simple novel prolate-oblate shape phase transitional description with a third order interaction term within the SU(3) limit for both the large-N limit and finite-N cases. The results indicate that the prolate-oblate phase transition shown in this description is of first-order due to the level-crossing, asymmetric with respect to values of the order parameters in the two phases, and well defined for finite-N cases. This novel prolate-oblate shape phase transitional description provides a simple completely solvable framework for the quantum phase transition in a finite-N system. Thus, it allows us to take a closer look at its critical behavior and study the N-dependent effects during the transition. Various finite-N effects on the shape phase transition were studied with the help of the correspondence between the shape variables in the finite-N cases and those defined by the coherent state theory. In contrast to the original SU(3)-O(6)-$\overline{\text{SU(3)}}$ shape phase transition [6, 25], the prolate-oblate phase transition discussed is asymmetric with respect to values of the order parameters in the two phases. The dynamical structure at the critical point is shown to be similar to but different from that in the O(6) symmetry [5], which is the critical point symmetry in the original SU(3)-O(6)-$\overline{\text{SU(3)}}$ description. In a comparison of our theoretical results for some shape-sensitive quantities compared with corresponding experimental data, the results show that the asymmetric prolate-oblate shape phase transitional description seems quite reasonable for a description of the ground state shape evolution with mass number A from ^{180}Hf to ^{198}Pt. Generally, besides terms with the SU(3) symmetry, other ingredients such as terms with the U(5) and O(6) symmetries may also need to be needed in order to fit experimental data quantitatively, and with

these the sudden change in the order parameters occurring at the critical point may be smoothed out due to the symmetry-mixing as the case in the original SU(3)-O(6)-$\overline{\text{SU(3)}}$ transitional description [6, 7, 25]. As reported in [43], a very tiny region of triaxiality can be found in the large-N limit around the critical point of the prolate-oblate phase transition when a more general IBM Hamiltonian involving the $[\hat{Q} \times \hat{Q} \times \hat{Q}]^{(0)}$ term is considered. According to the analysis in this work, triaxiality in finite-N cases seems also important since the characteristics of triaxiality may be magnified due to the finite-N effects [10, 24]. A discussion regarding the effective triaxial deformations induced by the finite-N effects has already been shown in [75]. In addition, similar SU(3) Hamiltonians to that given in (17) as well as more generalized forms were considered earlier by a number authors in the SU(3) shell model [35–40]. Our present investigation reveals such extension to the boson case is indeed feasible, which may provide additional insight into the SU(3) IBM theory from a more microscopic point of view [35].

In conclusion, the simple novel prolate-oblate shape phase transitional description presented in this work further enriches the IBM interpretation of nuclear shape phase and phase transitions. One can extend this scheme to the $\overline{\text{SU(3)}}$ description via the gauge transformation $s^\dagger \mapsto e^{i\pi} s^\dagger$, but the transitional mechanism remains the same, which derives from the fact that the effect is due to level-crossing when a third-order term is introduced. More general situations involving the U(5), O(6) symmetry terms, and the fourth order term necessary in describing a triaxial rotor may also be considered. Related work is in progress.

Acknowledgments

Support from the U.S. National Science Foundation (PHY-0500291 & OCI-0904874), the Southeastern Universities Research Association, the Natural Science Foundation of China (11005056, 11175078, 11075080, 10935001, and 11075052), the Major State Basic Research Development Program (G2007CB815000), the Doctoral Program Foundation of the State Education Ministry of China (20102136110002), and the LSU–LNNU joint research program (9961) is acknowledged.

[1] J. N. Ginocchio and M. W. Kirson, Phys. Rev. Lett. **44**, 1744 (1980).

[2] A. E. L. Dieperink, O. Scholten, and F. Iachello, Phys. Rev. Lett. **44**, 1747 (1980).

[3] D. H. Feng, R. Gilmore, and S. R. Deans, Phys. Rev. **C 23**, 1254 (1981).

[4] P. Van Isacker and J. Q. Chen, Phys. Rev. **C 24**, 684 (1981).

[5] F. Iachello and A. Arima, *The Interacting Boson Model* (Cambridge University, Cambridge, England, 1987).

[6] J. Jolie, R. F. Casten, P. von Brentano, and V. Werner, Phys. Rev. Lett. **87**, 162501 (2001).

[7] J. Jolie and A. Linnemann, Phys. Rev. **C 68**, 031301(R) (2003).

[8] J. Jolie, P. Cejnar, R. F. Casten, S. Heinze, A. Linnemann, and V. Werner, Phys. Rev. Lett. **89**, 182502 (2002).

[9] J. M. Arias, J. Dukelsky, and J. E. García-Ramos, Phys. Rev. Lett. **91**, 162502 (2003).

[10] F. Iachello and N. V. Zamfir, Phys. Rev. Lett. **92**, 212501 (2004).

[11] D. J. Rowe, Phys. Rev. Lett. **93**, 122502 (2004)

[12] D. J. Rowe, P. S. Turner, and G. Rosensteel, Phys. Rev. Lett. **93**, 232502 (2004).

[13] P. Cejnar, S. Heinze, and J. Dobeš, Phys. Rev. **C 71**, 011304(R) (2005).

[14] S. Dusuel, J. Vidal, J. M. Arias, J. Dukelsky, and J. E. García-Ramos, Phys. Rev. **C 72**, 064332 (2005).

[15] J. M. Arias, J. Dukelsky, J. E. García-Ramos, and J. Vidal, Phys. Rev. **C 75**, 014301 (2007).

[16] D. D. Warner and R. F. Casten, Phys. Rev. **C 28**, 1798 (1983).

[17] A. Leviatan, Phys. Rev. Lett. **77**, 818 (1996); **98**, 242502 (2007); A. Leviatan and P. Van Isacker, Phys. Rev. Lett. **89**, 222501 (2002).

[18] Y. X. Liu, L. Z. Mu, and H. Wei, Phys. Lett. **B 633**, 49 (2006).

[19] Y. Zhang, Z. F. Hou, H. Chen, H. Wei, and Y. X. Liu, Phys. Rev. **C 78**, 024314 (2008).

[20] Y. Zhang, Z. F. Hou, and Y. X. Liu, Phys. Rev. **C 76**, 011305(R) (2007).

[21] Z. P. Li, T. Nikšić, D. Vretenar and J. Meng, Phys. Rev. **C 80**, 061301(R) (2009).

[22] E. Lopez-Moreno and O. Castanos, Phys. Rev. **C 54**, 2374 (1996).

[23] E. Lopez-Moreno and O. Castanos, Rev. Mex. Fis. **44**, 48 (1998).

[24] F. Pan, J. P. Draayer, and Y. Luo, Phys. Lett. **B 576**, 297 (2003).

[25] F. Pan, T. Wang, Y. S. Huo, and J. P. Draayer, J. Phys. **G 35**, 125105 (2008).

[26] P. Cejnar, S. Heinze, and J. Jolie, Phys. Rev. **C 68**, 034326 (2003).

[27] R. F. Casten and E. A. McCutchan, J. Phys. **G 34**, R285 (2007).

[28] P. Cejnar and J. Jolie, Prog. Part. Nucl. Phys. **62**, 210 (2009).

[29] P. Cejnar, J. Jolie and R. F. Casten, Rev. Mod. Phys. **82**, 2155 (2010).

[30] D. Kusnezov, Phys. Rev. Lett. **79**, 537 (1997).

[31] A. M. Shirokov, N. A. Smirnova, and Y. F. Smirnov, Phys. Lett. **B 434**, 237 (1998).

[32] K. Heyde, P. Van Isacker, M. Waroquier, and J. Moreau, Phys. Rev. **C 29**, 1420 (1984).

[33] P. Van Isacker, Phys. Rev. Lett. **83**, 4269 (1999).

[34] Yu. F. Smirnov, N. A. Smirnova, and P. Van Isacker, Phys. Rev. **C 61**, 041302(R) (2000).

[35] J. P. Draayer and G. Rosensteel, Nucl. Phys. **A 439**, 61 (1985).

[36] Y. Leschber and J. P. Draayer, Phys. Rev. **C 33**, 749 (1986).

[37] J. Carvalho, R. Le Blanc, M. Vassanji, D. J. Rowe, and J. M. McGrory, Nucl. Phys. **A 452**, 240 (1986).

[38] P. Rochford and D. J. Rowe, Phys. Lett. **B 210**, 5 (1988).

[39] O. Castaños, J. P. Draayer, and L. Leschber, Z. Phys. **A 329**, 33 (1988).

[40] C. Bahri, J. Escher, and J. P. Draayer, Nucl. Phys. **A 592**, 171 (1995).

[41] G. Vanden Berghe, H. E. De Meyer, and P. Van Isacker, Phys. Rev. **C 32**, 1049 (1985).

[42] J. Vanthournout, Phys. Rev. **C 41**, 2380 (1990).

[43] L. Fortunato, C. E. Alonso, J. M. Arias, J. E. Garcìa-Ramos, and A. Vitturi, Phys. Rev. **C 84**, 014326 (2011).

[44] P. Van Isacker, A. Frank, and J. Dukelsky, Phys. Rev. **C 31**, 671 (1985).

[45] P. Cejnar and J. Jolie, Phys. Lett. **B 420**, 241 (1998).

[46] J. P. Elliott, Proc. Roy. Soc. **A 245**, 128, 562 (1958).

[47] J. D. Vergados, Nucl. Phys. **A 111**, 681 (1968).

[48] G. Rosensteel, Phys. Rev. **C 41**, 730 (1990).

[49] J. P. Draayer and Y. Akiyama, J. Math. Phys. **14**, 1904 (1973).

[50] Y. Akiyama and J. P. Draayer, Comput. Phys. Commun. **5**, 405 (1973).

[51] P. Cejnar and J. Jolie, Phys. Rev. **E 58**, 387 (1998).

[52] D. Bonatsos, E. A. McCutchan, and R. F. Casten, Phys. Rev. Lett. **101**, 022501 (2008).

[53] D. Bonatsos, E. A. McCutchan, R. F. Casten, R. J. Casperson, V. Werner, and E. Williams, Phys. Rev. **C 80**, 034311 (2009).

[54] P. Cejnar and P. Stràns kỳ, Phys. Rev. **E 78**, 031130 (2008).

[55] M. A. Caprio, P. Cejnar and F. Iachello, Ann. Phys. **323**, 1106 (2008).

[56] V. Werner, C. Scholl, and P. von Brentano, Phys. Rev. **C 71**, 054314 (2005).

[57] S. Raman, C. W. Nestor, and P. Tikkanen, Atom. Data Nucl. Data Tables **78**, 1 (2001).

[58] P. Möller, J. R. Nix, W. D. Myers, and W. J. Swiatecki, Atom. Data Nucl. Data Tables **59**, 185 (1995).

[59] K. Kumar, Phys. Rev. **C 1**, 369 (1970).

[60] S. C. Wu and H. Niu, Nucl. Data Sheets **100**, 483 (2003).

[61] B. Singh and J. C. Roediger, Nucl. Data Sheets **111**, 2081 (2010).

[62] C. M. Baglin, Nucl. Data Sheets **111**, 275 (2010).

[63] C. M. Baglin, Nucl. Data Sheets **99**, 1 (2003).

[64] B. Singh, Nucl. Data Sheets **95**, 387 (2002).

[65] B. Singh, Nucl. Data Sheets **99**, 275 (2003).

[66] C. M. Baglin, Nucl. Data Sheets **84**, 717 (1998).

[67] B. Singh, Nucl. Data Sheets **107**, 1531 (2006).

[68] X. L. Huang, Nucl. Data Sheets **108**, 1093 (2007).

[69] X. L. Huang, Nucl. Data Sheets **110**, 2533 (2009).

[70] W. Greiner and J. A. Maruhn, *Nuclears Models* (Springer-Verlag Berlin 1996).

[71] A. S. Davydov and B. F. Filippov, Nucl. Phys. **8**, 237 (1958).

[72] R. Fossion, Dennis Bonatsos, and G. A. Lalazissis, Phys. Rev. **C 73**, 044310 (2006).

[73] P. Sarriguren, R. Rodríguez-Guzmán, and L. M. Robledo Phys. Rev. **C 77**, 064322 (2008).

[74] K. Nomura, T. Otsuka, R. Rodríguez-Guzmán, L. M. Robledo, and P. Sarriguren, Phys. Rev. **C 84**, 054316 (2011).

[75] O. Castaños, A. Frank, and P. Van Isacker, Phys. Rev. Lett. **52**, 263 (1984).